



A Flexible Network of Lipid Droplet Associated Proteins Support Embryonic Integrity of *C. elegans*

Zhe Cao, Chun Wing Fung and Ho Yi Mak^{*†}

Division of Life Science, The Hong Kong University of Science and Technology, Hong Kong SAR, China

OPEN ACCESS

Edited by:

Vineet Choudhary,
All India Institute of Medical Sciences,
India

Reviewed by:

Toyoshi Fujimoto,
Juntendo University, Japan
Hanaa Hariri,
Wayne State University, United States

*Correspondence:

Ho Yi Mak
hym@ust.hk

†ORCID:

Ho Yi Mak
orcid.org/0000-0002-1500-5328

Specialty section:

This article was submitted to
Membrane Traffic,
a section of the journal
Frontiers in Cell and Developmental
Biology

Received: 17 January 2022

Accepted: 16 March 2022

Published: 04 April 2022

Citation:

Cao Z, Fung CW and Mak HY (2022) A
Flexible Network of Lipid Droplet
Associated Proteins Support
Embryonic Integrity of *C. elegans*.
Front. Cell Dev. Biol. 10:856474.
doi: 10.3389/fcell.2022.856474

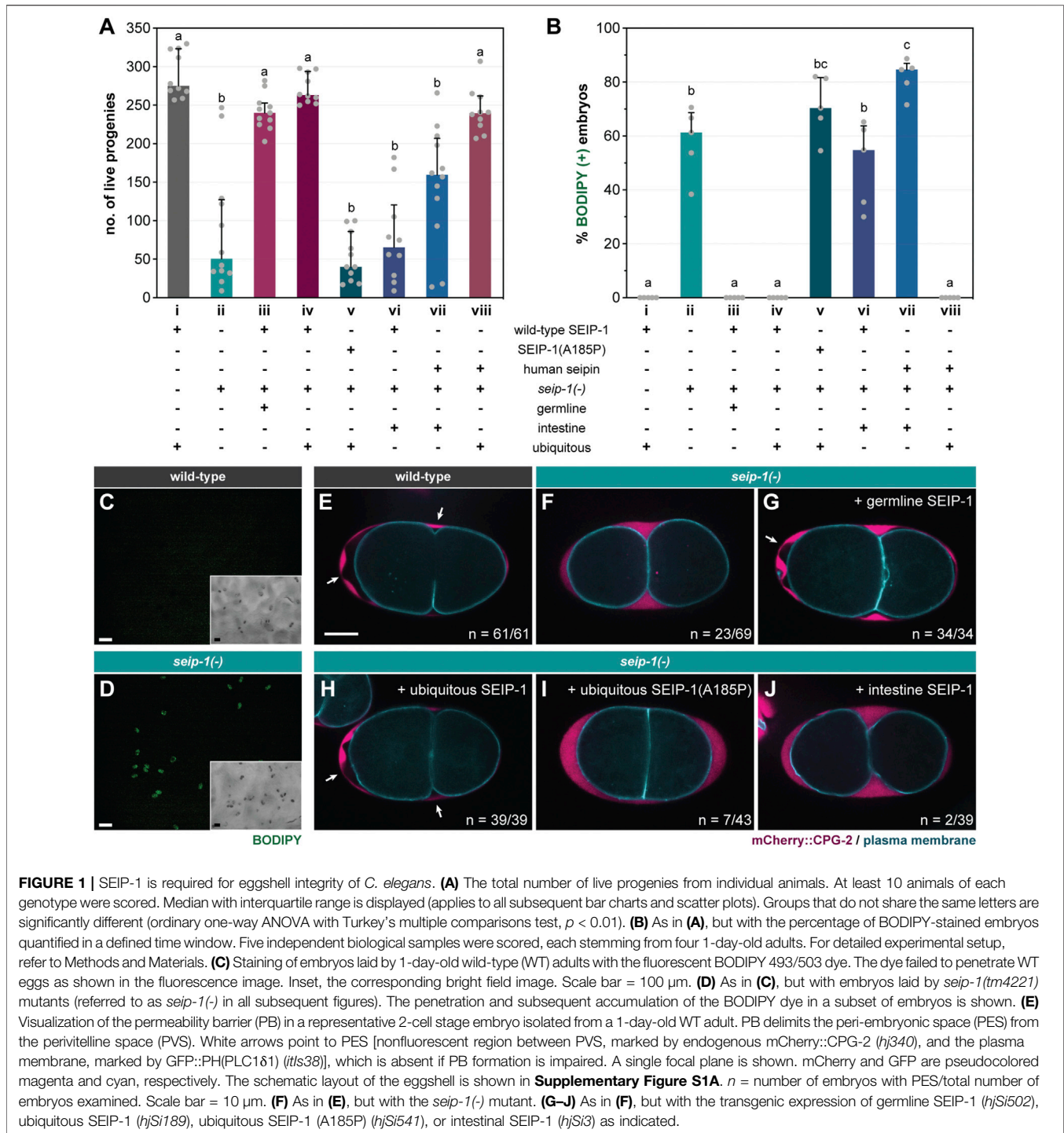
In addition to coordinating the storage and mobilization of neutral fat, lipid droplets (LDs) are conserved organelles that can accommodate additional cargos in order to support animal development. However, it is unclear if each type of cargo is matched with a specific subset of LDs. Here, we report that SEIP-1/seipin defines a subset of oocyte LDs that are required for proper eggshell formation in *C. elegans*. Using a photoconvertible fluorescent protein-based imaging assay, we found that SEIP-1 positive LDs were selectively depleted after fertilization, coincident of the formation of a lipid-rich permeability barrier of the eggshell. Loss of SEIP-1 function caused impenetrant embryonic arrest, which could be worsened by FAT-3/fatty acyl-CoA desaturase deficiency or suppressed by PLIN-1/Perilipin deficiency. The embryonic development of *seip-1*; *plin-1* mutant in turn depended on the recruitment of RAB-18/Rab18 to LDs, which was not observed in wild type embryos. We propose that SEIP-1 dependent and independent mechanisms act in parallel to ensure the packaging and export of lipid-rich permeability barrier constituents, which involve LDs. The identity of these LDs, as defined by their associated proteins, exhibits unexpected plasticity that ultimately ensures the survival of embryos *ex utero*.

Keywords: seipin, SEIP-1, lipid droplets, perilipin, Rab18

INTRODUCTION

The deposition of fat is an essential process in the maturation of female germ cells in animals. Such maternal contribution of fat provides energy and membrane precursors that support early embryonic development. Accordingly, lipid droplets (LDs), which are evolutionarily conserved organelles that coordinate fat storage and utilization, are readily detected in vertebrate and invertebrate oocytes and embryos (Welte, 2015; Chen et al., 2020; Ibayashi et al., 2021; Mosquera et al., 2021). The structure of LDs are distinct from other intracellular organelles because a phospholipid monolayer serves as the delimiting membrane (Tauchi-Sato et al., 2002; Walther et al., 2017; Olzmann and Carvalho, 2019). This has led to a model that LDs bud from the outer leaflet of the endoplasmic reticulum (ER) and maintain contact with the ER *via* protein- and membrane-bridges. The core of LDs contains neutral lipids, such as triacylglycerol (TAG) or cholesterol ester. It is known that the composition of the neutral lipid core varies in a cell type- and nutrient-dependent manner, which in part reflects the demand and supply of specific lipid species (Fu et al., 2014; Molenaar et al., 2021).

Recent evidence suggests that subpopulations of LDs within a single cell can be further distinguished by their association with metabolic enzymes or ER subdomains (Wilfling et al., 2013; Thul et al., 2017; Cao et al., 2019). For example, a subset of LDs in the *C. elegans* intestinal cells associate with a tubular ER-subdomain, defined by the preferential enrichment of the seipin ortholog, SEIP-1 (Cao et al., 2019). Such enrichment is dependent on endogenous



polyunsaturated fatty acids and cyclopropane fatty acids that are derived from the bacterial diet, hinting at a link between specific fatty acid availability and LD diversity. In humans, recessive loss-of-function mutations in seipin cause generalized lipodystrophy, which has been attributed to its role in supporting LD biogenesis and expansion (Magré et al., 2001; Payne et al., 2008; Cartwright and Goodman, 2012; Chen et al., 2012; Salo et al., 2016; Wang et al., 2016). In *C. elegans*, the loss of SEIP-1 function reduces the

size of a subset of LDs in intestinal cells and perturbs eggshell formation and embryonic development (Cao et al., 2019; Bai et al., 2020). Thus far, it is not completely understood how seipin deficiency at the subcellular level contributes to diverse phenotypes at the organismal level.

The eggshell formation of *C. elegans* is a hierarchical process that demands the sequential secretion of protein- and lipid-rich material into the extracellular space after fertilization (**Supplementary Figure**

S1A) (Johnston and Dennis, 2012; Olson et al., 2012; Stein and Golden, 2018). The eggshell protects the embryo from mechanical and osmotic shock to ensure proper development after its expulsion from the mother. Specifically, the lipid-rich layer of the eggshell serves as a permeability barrier that prevents uncontrolled influx of water. Based on genetic analysis, it has been proposed that the permeability barrier is composed of ascarosides, which are sugar-fatty acid conjugates (Olson et al., 2012). However, it is unclear how ascarosides are packaged and exported from the zygote.

In this paper, we investigated the role of SEIP-1 in supporting permeability barrier formation. Similar to intestinal cells, we observed a subset of oocyte and embryonic LDs that were surrounded by SEIP-1 positive ER. Loss of *seip-1* function conferred an impenetrant embryonic arrest phenotype. Paradoxically, such phenotype could be suppressed by the loss of specific LD-associated proteins. We propose that multiple ensembles of LD-associated proteins support parallel mechanisms for LDs to accept specialized cargoes. In *C. elegans* oocytes, such SEIP-1 dependent and independent mechanisms presumably ensure the packaging of ascarosides in LDs prior to their export, which is vital for the construction of the eggshell permeability barrier.

RESULTS AND DISCUSSION

Loss of SEIP-1 Function Causes Impenetrant Embryonic Arrest

The *seip-1(tm4221)* deletion allele [*seip-1(-)* thereafter] was initially annotated as lethal by the National Bioresource Project (Mitani, 2017). Surprisingly, upon outcrossing with wild type worms, we discovered that *seip-1(-)* worms were fertile (median = 51 live progenies per animal) (column ii, **Figure 1A**). The significant reduction in viable progeny was due to a large number of eggs that failed to hatch after being laid. In a separate attempt to study the lipid accumulation of *seip-1(-)* worms, we cultured them in the presence of the vital dye BODIPY on standard nematode growth media (NGM) plates. Although the total number of eggs laid by wild type and *seip-1(-)* worms were comparable (**Supplementary Figure S1B**), BODIPY could not penetrate wild type eggs, while ~60% of *seip-1(-)* eggs were stained (**Figures 1B–D**). The strong correlation between BODIPY staining and embryonic arrest suggested that the latter might be caused by a structural deficiency of the eggshell (**Supplementary Figure S1A**). Consequently, the penetration of exogenous material might interfere with embryonic development. Because some *seip-1(-)* embryos develop and hatch as L1 larvae, we therefore conclude that SEIP-1 acts in parallel of additional proteins to ensure embryonic viability. Interestingly, *seip-1(-)* eggs laid by relatively young adults were more prone to BODIPY staining (**Supplementary Figure S1C**). Therefore, it is plausible that the SEIP-1-independent mechanism is triggered at least 1 day after the initiation of egg laying.

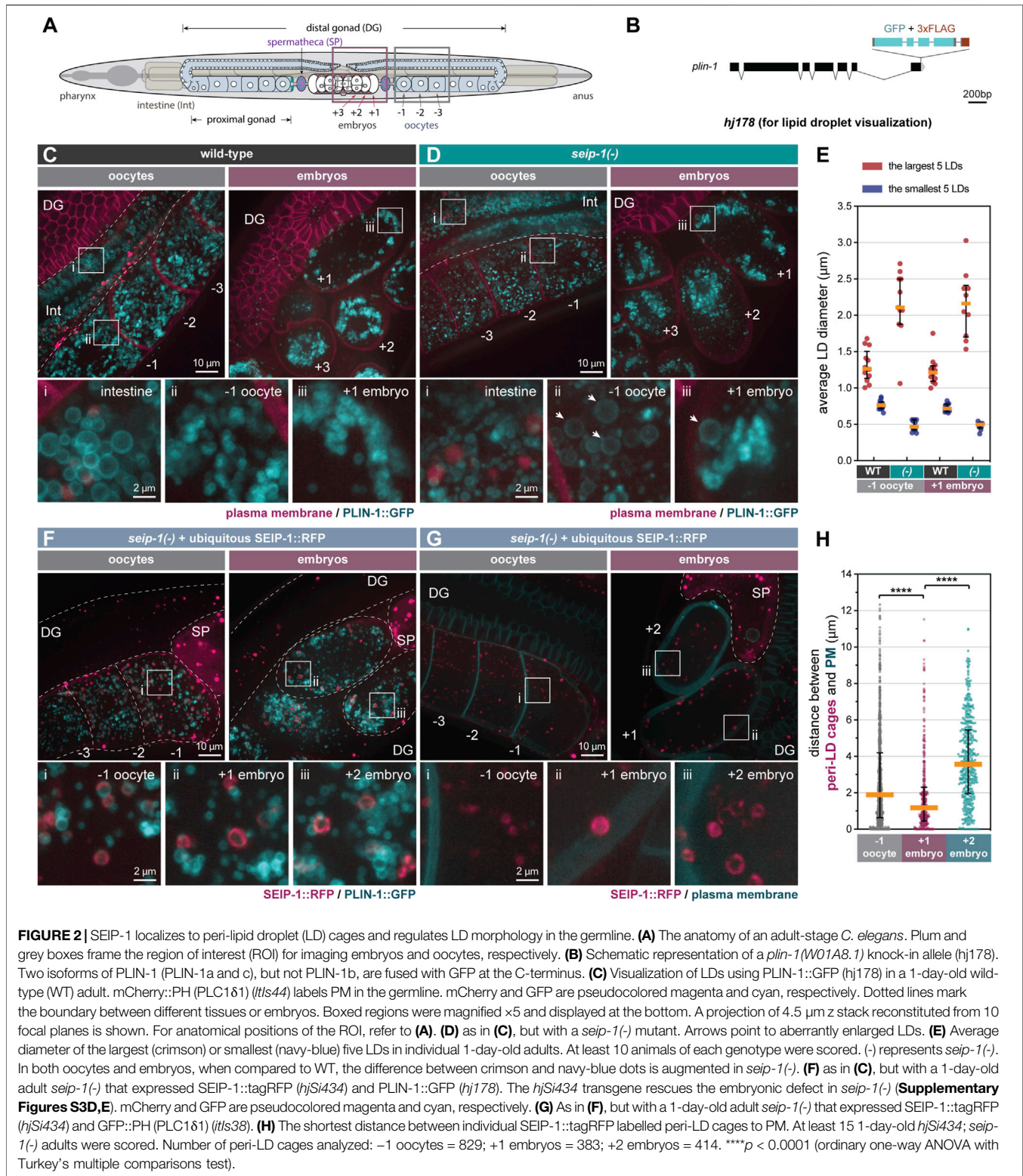
A Subpopulation of *seip-1(-)* Embryos Lack the Permeability Barrier

The structural integrity of the *C. elegans* eggshell is critical for embryonic development, because defects in the eggshell can cause

mitotic and polarity defects (Olson et al., 2012). Upon fertilization of the oocyte in the spermatheca, the *C. elegans* eggshell is formed by the hierarchical establishment of four discrete protein- or lipid-rich layers. Starting with the outermost vitellin layer (VL), the chitin layer (CL), the chondroitin proteoglycan layer (CPG), and the permeability barrier were sequentially formed toward the embryonic plasma membrane (**Supplementary Figure S1A**). We noted that the embryonic arrest phenotype of *seip-1(-)* worms was similar to a class of mutants that fail to form the permeability barrier properly. Accordingly, a large number of *perm-1* and *dgtr-1* embryos could be stained when they were laid on BODIPY-containing NGM plates (**Supplementary Figure S1D**). The permeability barrier separates the perivitelline space and the peri-embryonic space (PES) (**Supplementary Figure S1A**). In wild type worms, the permeability barrier retains the chondroitin proteoglycan CPG-2 in the perivitelline space and exclude it from the peri-embryonic space (**Figure 1E**). In contrast, we found abnormal accumulation of CPG-2 near the plasma membrane in a fraction of *seip-1(-)* embryos (**Figure 1F**), similar to *perm-1* and *dgtr-1* deficient embryos (Olson et al., 2012). Live imaging of wild type embryos *in utero* indicated the emergence of PES upon the cortical ruffling of plasma membrane (**Supplementary Video S1**) (Green et al., 2008). PES expands during the pseudocleavage (Goldstein et al., 1993) and is likely finalized following the first mitotic cleavage, which results in two-cell-stage embryos (**Supplementary Video S1**). In contrast, PES failed to emerge even after the first mitotic cleavage of some *seip-1(-)* embryos, whereas the exocytosis of CPG-2 was unperturbed (**Supplementary Video S2**). Our results are consistent with a recent report (Bai et al., 2020), and implied that SEIP-1 is necessary for the proper formation of the permeability barrier, but not other layers of the eggshell.

A Lipodystrophy-Associated Mutation at a Conserved Residue Impairs SEIP-1 Function

The Alanine 212 to Proline (A212P) mutation in human seipin causes congenital generalized lipodystrophy type 2 disease (CGL2) (Magré et al., 2001). Based on primary sequence alignment, we noted that A185 of SEIP-1 is orthologous to A212 of human seipin (**Supplementary Figure S2A**). To assess if the conserved alanine is important for SEIP-1 function, we generated single-copy transgenes that expressed either SEIP-1 (wild-type)::GFP (*hjSi189*) or SEIP-1 (A185P)::GFP (*hjSi541*), driven by the ubiquitous *dpy-30* promoter. Wild type SEIP-1::GFP supported the formation of the embryonic permeability barrier (**Figure 1H**) and restored the fertility of *seip-1(-)* mutants (**Figure 1A**, column iv). Correspondingly, no BODIPY-stained embryos were observed (**Figure 1B**, column iv). In contrast, SEIP-1 (A185P) failed to suppress the permeability barrier defects of *seip-1(-)* mutant worms (**Figures 1A,I**, column v; **Figure 1B**, column v). To complement our single-copy transgene strategy, we engineered a knock-in *seip-1(A185P)* allele (*hj158*) using CRISPR. Based on our homology directed repair (HDR) methodology, an “orphan”



loxP sequence was inserted between the stop codon and 3'-UTR of *seip-1*(*A185P*) (**Supplementary Figure S2B**). We therefore constructed a control wild-type *seip-1* allele (*hj156*) with a loxP site inserted at the same position as in *hj158* (**Supplementary**

Figure S2B). The fertility of *seip-1*(*hj156*) animals was comparable to that of wild type. However, the fertility of *seip-1*(*hj158*) (i.e., *A185P*) was reduced to a level similar to *seip-1*(-) animals, with a corresponding increase in BODIPY-positive

embryos (**Supplementary Figures S2C,D**). Our observations were consistent with those made using an independently generated allele that encoded SEIP-1 (A185P) (Bai et al., 2020). We conclude that the A185P mutation disrupts SEIP-1 function, similar to the effect of A212P to human seipin.

Expression of SEIP-1 in the Germline Supports Embryonic Development

Endogenous SEIP-1 is expressed in both the intestine and the germline (Cao et al., 2019; Bai et al., 2020). In *C. elegans*, the proper embryonic development is dependent on the supply of intestine-derived yolk proteins (Grant and Hirsh, 1999; Ezcurra et al., 2018). To this end, we sought to determine the site of SEIP-1 action for proper embryogenesis. Germline-specific expression of SEIP-1 with the *sun-1* promoter (*hjSi502*) fully rescued the defect of *seip-1(-)* embryos (**Figure 1B, column iii; Figure 1G**), thereby restoring the fertility of *seip-1(-)* worms to the wild-type level (**Figure 1A, column iii**). In contrast, intestine-specific expression of SEIP-1 with the *vha-6* promoter (*hjSi3*) did not rescue the embryonic defect (**Figure 1B, column vi; Figure 1J, column vi**) or the fertility of *seip-1(-)* mutants (**Figure 1A, column vi**). Similarly, ubiquitous but not intestine-specific expression of human seipin rescued the defects of *seip-1(-)* embryos (**Figure 1A, columns vii and viii; Figure 1B, columns vii and viii**). Taken together, a conserved function of SEIP-1/seipin is required in the germline to support embryonic development.

SEIP-1 Regulates LD Morphology in the Germline

We previously demonstrated that SEIP-1 regulates intestinal LD expansion (Cao et al., 2019), using the mRuby-tagged *C. elegans* diacylglycerol *O*-acyltransferase 2 ortholog, DGAT-2 (Xu et al., 2012), as the LD marker. Prompted by the germline-specific function of SEIP-1, we examined the morphology of germline LDs in *seip-1(-)* worms. Because DGAT-2 is primarily found in intestinal cells, we needed an alternative marker to visualize germline LDs. To this end, we used the sole *C. elegans* perilipin ortholog, MDT-28/PLIN-1 (for simplicity, referred to as PLIN-1 in subsequent text), which is ubiquitously expressed (Na et al., 2015). We engineered a knock-in allele (*hj178*) for which the two long isoforms of PLIN-1 (PLIN-1a/c) were tagged with GFP at their C-termini (**Figure 2B**). Consistent with our previous finding, intestinal PLIN-1-labeled LDs in *seip-1(-)* worms were smaller than those in wild type worms (**Figures 2C,D, inset i**). Surprisingly, in contrast to the more uniformly sized LDs in the wild-type germline (**Figure 2C**), we found abnormally large or small LDs in both oocytes (inset ii) and embryos (inset iii) of *seip-1(-)* mutants (**Figure 2D**). As a result, the size range of LDs in *seip-1(-)* germline was larger than that in wild type (**Figure 2E**). We made similar observations in *seip-1(A185P)* loss of function mutants (**Supplementary Figures S2E–G**). Such aberrant LD morphology in the SEIP-1 deficient germline is reminiscent of that in yeast and cell line models when seipin orthologs are depleted (Szymanski et al., 2007; Fei et al., 2008; Salo et al., 2016; Wang et al., 2016; Chung et al., 2019). Our

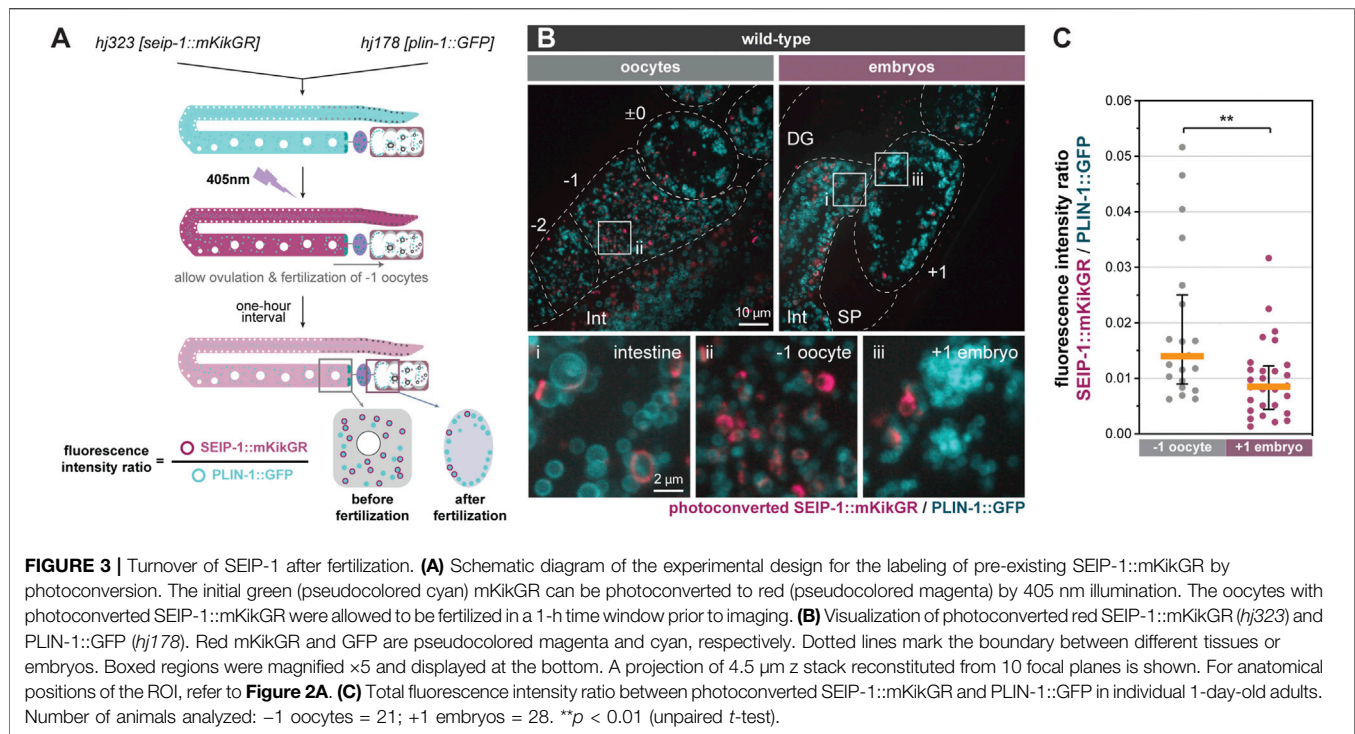
results indicate that seipin deficiency causes distinct LD defects in proliferating versus differentiated cells (such as *C. elegans* intestinal cells).

Germline SEIP-1 Localizes to Peri-LD Cages

SEIP-1 is enriched at a subdomain of the endoplasmic reticulum (ER), termed the peri-LD cage (Cao et al., 2019), in the *C. elegans* intestine. To investigate the localization of SEIP-1 in the germline, we first examined SEIP-1(WT)::GFP in adult worms that lacked the endogenous SEIP-1 protein. In both oocytes and embryos, SEIP-1(WT)::GFP was targeted to “ring” or “cage”-like structures (**Supplementary Figure S3A**). Similar observations were made in *seip-1(-)* worms that expressed human seipin::GFP ubiquitously (**Supplementary Figure S3C**). In comparison, SEIP-1 (A185P)::GFP was rarely found in equivalent structures (**Supplementary Figure S3B**). Such localization defect might be linked to its reduced oligomeric state, as reported for human seipin (A212P) (Binns et al., 2010; Sui et al., 2018; Yan et al., 2018). Next, we examined the localization of a SEIP-1::tagRFP fusion protein, relative to the PLIN-1::GFP LD marker. We reasoned that the SEIP-1::tagRFP fusion protein, expressed from a single-copy transgene (*hjSi434*), was functional since it could rescue both the fertility and the permeability barrier defect of *seip-1(-)* worms (**Supplementary Figures S3D,E**). SEIP-1::tagRFP was enriched in tubular structures around a subset of PLIN-1 positive LDs in the germline (**Figure 2F**). Therefore, SEIP-1 appeared to mark a subset of LDs in the germline, similar to our previous observations in the intestine. Additional subcellular compartments, such as cortical granules (Bembenek et al., 2007; Olson et al., 2012) and yolk particles (Sharrock et al., 1990) are known to contribute to early embryogenesis and their reported sizes are similar to that of LDs. Therefore, we asked if SEIP-1 could be found in the proximity of these structures. The cortical granules are exocytosed by canonical anterograde trafficking (Bembenek et al., 2007). They can be marked with COPII components. We focused on SEC-16A.1, which is one of the 2 *C. elegans* orthologs of mammalian and yeast SEC16 that is found at ER-exit sites (ERES) and COPII vesicles (Watson et al., 2006). Accordingly, we constructed a knock-in allele that expressed SEC-16A.1 with a C-terminal GFP tag (**Supplementary Figure S3F**). For the visualization of yolk particles, we used a published knock-in allele that expressed VIT-2::GFP (Perez et al., 2017). Overall, we did not observe overt colocalization of SEIP-1 and SEC-16A.1 or VIT-2 in oocytes or embryos (**Supplementary Figures S3G,H**). Our results imply that LDs associated with SEIP-1 (+) cages are distinct from other vesicular structures such as cortical granules and yolk particles.

Enrichment of SEIP-1 (+) LDs Near the Plasma Membrane Upon Fertilization

We next sought to understand how SEIP-1 (+) LDs might regulate the formation of the permeability barrier. Based on live imaging, we consistently observed LDs and SEIP-1-labeled peri-LD cages near the cell cortex of +1 embryos, but not in –1



oocytes or +2 embryos (**Figures 2A,C,F,G, Supplementary Video S3**). To quantify this phenomenon, we compared the localization of SEIP-1 relative to the plasma membrane (**Figure 2G**) by measuring the shortest distance from each peri-LD cage to the plasma membrane in cells at either -1, +1, or +2 position. The median distance was reduced from $\sim 2 \mu\text{m}$ in -1 oocytes and $\sim 3.8 \mu\text{m}$ in +2 embryos to $\sim 1 \mu\text{m}$ in +1 embryos (**Figure 2H**). In sum, our data is consistent with a model that upon fertilization, SEIP-1 (+) LDs are recruited to the cortical region of the zygote to support the formation of permeability barrier. Such distribution pattern of SEIP-1 was not observed in the differentiated intestine (Cao et al., 2019), again highlighting the distinct function of SEIP-1 positive structures in proliferating versus differentiated cells.

SEIP-1 (+) LDs Preferentially Disappeared During the Construction of the Permeability Barrier

We hypothesized that the redistribution of SEIP-1 (+) LDs near the plasma membrane supports the construction of the permeability barrier in newly fertilized embryos. To determine if such redistribution is linked to the catabolism or anabolism of SEIP-1 (+) LDs, we developed a photoconversion strategy to label preexisting SEIP-1 in the oocytes. From the endogenous *seip-1* locus, we expressed the fusion of the monomeric photoconvertible fluorescent protein mKikGR (Habuchi et al., 2008) with SEIP-1 (SEIP-1::mKikGR). In the same worms, we also expressed the ubiquitous LD marker, PLIN-1::GFP. When one-day-old adult worms were exposed to 405 nm fluorescence, all green SEIP-1::mKikGR fusion proteins in the germline were

converted to red (pseudocolored magenta) (**Figure 3A**). These worms were subsequently examined after a 1-h lag. This lag was necessitated when the following events were taken into consideration: ovulation cycle (~ 15 min) (Huelgas-Morales and Greenstein, 2018), fertilization in the spermatheca (~ 5 min), and development from fertilization to the first mitotic division (40 min) (Stein and Golden, 2018). Therefore, by the time of imaging, the formation of the permeability barrier and the presumptive turnover of oocyte-derived SEIP-1::mKikGR should be complete in +1 embryos. Consistent with our previous study with single-copy transgenes (Cao et al., 2019), endogenous SEIP-1::mKikGR was also targeted to peri-LD cages in the intestine (**Figure 3B**, inset i). In the germline, we found fewer pre-existing, photoconverted peri-LD cages in +1 embryos than in -1 oocytes (**Figure 3B**, inset ii and iii). Such reduction correlated with a decrease in the photoconverted SEIP-1::mKikGR to PLIN-1::GFP fluorescence intensity ratio (**Figures 3A,C**). In this case, PLIN-1::GFP fluorescence was used for normalization across different +1 embryos. Altogether, we propose that SEIP-1 (+) LDs mobilization to the plasma membrane and their subsequent disappearance are integral steps of permeability barrier formation.

A genetic pathway, consisting of FASN-1, POD-2, PERM-1, and DGTR-1, has previously been shown to control permeability barrier formation (Olson et al., 2012; Stein and Golden, 2018). How does SEIP-1 fit into such pathway? Interestingly, the terminal enzyme DGTR-1 is a germline-specific paralog of DGAT-2, which contributes to neutral lipid synthesis in the intestine. We propose that the lipid cargoes, synthesized by DGTR-1, for constructing the permeability barrier are contained in germline LDs. Notably, FASN-1, POD-2, PERM-

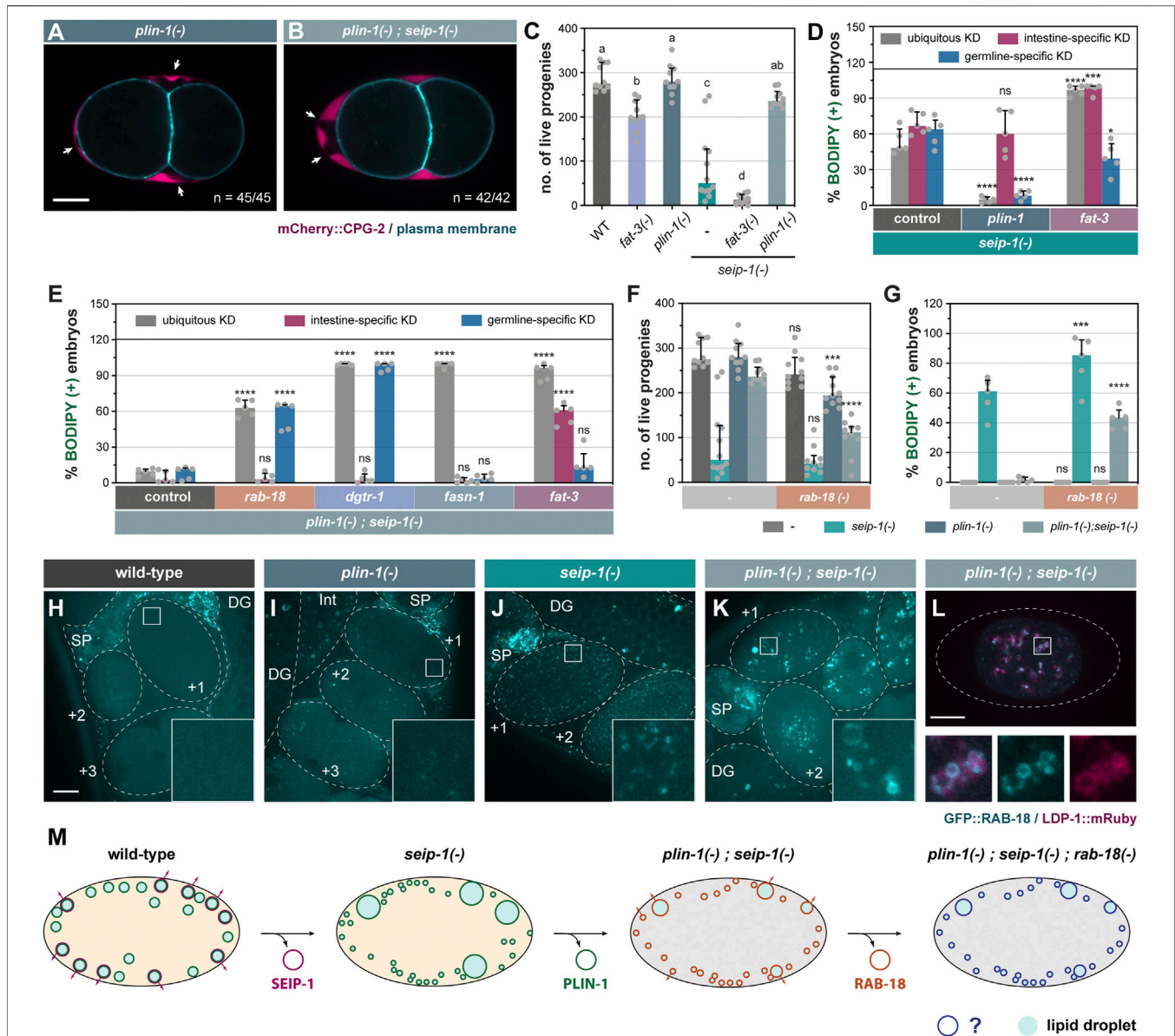


FIGURE 4 | Genetic modifiers of *seip-1(-)* delineate a parallel pathway for eggshell integrity. **(A)** Visualization of PB in a representative 2-cell stage embryo isolated from a 1-day-old *plin-1(tm1704)* (referred as *plin-1(-)* in all subsequent figures) null adult. White arrows point to PES. A single focal plane is shown. mCherry and GFP are pseudocolored magenta and cyan, respectively. n = number of embryos with PES/total number of embryos examined. Scale bar = 10 μ m. **(B)** as in **(A)**, but with *plin-1(-); seip-1(-)* double mutant. **(C)** The total number of live progenies from individual animals. At least 10 animals of each genotype were scored. Groups that do not share the same letters are significantly different (ordinary one-way ANOVA with Turkey's multiple comparisons test, $p < 0.01$). **(D)** The percentage of BODIPY-stained embryos with individual genes knocked down in the specified tissues of *seip-1(-)* mutant animals. For every knockdown condition, five independent repeats were scored, each with progeny from four adults. For detailed experimental setup, refer to Methods and Materials. Statistical significance on top of each bar was calculated by comparing each experimental group with its counterpart in the control group (RNAi vector) (two-way ANOVA with Sidak's multiple comparisons test). * $p < 0.05$, **** $p < 0.0001$. **(E)** as in **(D)**, but with tissue-specific RNAi in *plin-1(-); seip-1(-)* background. **(F)** as in **(C)**, but with animals carrying the *rab-18(ok2020)* [hereafter refer to as *rab-18(-)*] allele in the indicated genetic backgrounds. Statistical significance was calculated by comparing each experimental group [with *rab-18(-)*] with its counterpart in the control group [without *rab-18(-)*] (two-way ANOVA and Sidak's multiple comparisons test). ns, not significant; *** $p < 0.001$; **** $p < 0.0001$. **(G)** as in **(F)**, but with the percentage of BODIPY-stained embryos shown. Data of the control groups in **(C)**, **(F)** and **(G)** were reproduced from **Figures 1A,B** as the measurement was all performed at the same time. **(H)** Visualization of GFP::RAB-18 expressed from its endogenous locus (*hj347*) in an otherwise wild-type 1-day-old adult. Dotted lines mark the boundary between different tissues or embryos. Boxed regions were magnified $\times 5$ and shown in the inset. GFP is pseudocolored cyan. A projection of 4.5 μ m z stack reconstituted from 10 focal planes is shown. Scale bar = 10 μ m. **(I)** as in **(G)**, but in *plin-1(-)* mutant background. **(J)** as in **(G)**, but in *seip-1(-)* mutant background. **(K)** as in **(G)**, but in *plin-1(-); seip-1(-)* mutant background. **(L)** Visualization of GFP::RAB-18 (*hj347*) and LDP-1::mRuby (*hj289*) in an isolated one-cell stage embryo from a 1-day-old *plin-1(-); seip-1(-)* adult. Dotted lines illustrate the boundary of the embryo. LDP-1::mRuby serves as a LD marker. GFP and mRuby are pseudocolored cyan and magenta, respectively. A single focal plane is shown. The boxed region was magnified $\times 4$ and shown at the bottom. **(M)** A model on how a flexible network of LD-associated proteins supports embryonic integrity. For all fluorescence images, a projection of 4.5 μ m z stack reconstituted from 10 focal planes is shown, scale bar = 10 μ m.

1 or DGTR-1 deficiency causes embryonic lethality at high penetrance (Tagawa et al., 2001; Carvalho et al., 2011), unlike SEIP-1 deficiency (Figures 1A,B). It is plausible that SEIP-1 acts downstream of the cargo synthesis enzymes by specifying a subset of LDs that are destined to be utilized for constructing the permeability barrier.

Differential Requirement for PUFAs in the Construction of the Permeability Barrier

We next sought to understand the molecular basis of incomplete penetrance and high variability of the embryonic defect of *seip-1(-)* worms (Figures 1A–F, Supplementary Figure S1C). FAT-3, a polyunsaturated fatty acyl-CoA (PUFA) desaturase, is required for targeting SEIP-1 to peri-LD cages in the intestine (Cao et al., 2019) and oocytes (Supplementary Figures S6A,B). Thus, FAT-3 products such as gamma linolenic acid (GLA, C18:3n6) and their derivatives appeared to be broadly required for the recruitment of SEIP-1 to peri-LD cages. Intriguingly, dietary GLA supplementation was reported to significantly rescue the permeability barrier defect of *seip-1(-)* worms (Bai et al., 2020), suggesting that GLA also boosts the function of a SEIP-1-independent pathway. To this end, we asked if FAT-3 deficiency could modify the phenotypes of *seip-1(-)* worms. Indeed, FAT-3 deficiency reduced the fertility of otherwise wild type worms or *seip-1(-)* worms (Figure 4C). Accordingly, *seip-1(-); fat-3(-)* worms displayed a highly penetrant embryonic arrest phenotype, similar to *dgtr-1* or *perm-1* deficient worms. We conclude that FAT-3 products and their derivatives are important for both SEIP-1-dependent and SEIP-1-independent pathways that are responsible for permeability barrier formation. Both pathways are blocked in *seip-1(-); fat-3(-)* worms.

Next, we expanded our analysis by comprehensively interrogating genes that regulate fatty acid (FA) synthesis and desaturation (Supplementary Figure S4A). The percentage of BODIPY-stained embryos (i.e., embryos with defective permeability barrier) was compared after individual genes were depleted by RNAi-based knockdown (KD). In *seip-1(-)* background, ubiquitous depletion of either *fat-3* or *fat-4* increased the number of embryos with permeability barrier defects (Supplementary Figure S4B). Accordingly, depleting enzymes upstream of FAT-3/FAT-4 (i.e., FAT-2, FAT-6, ELO-1, and ELO-2) enhanced the embryonic arrest of *seip-1(-)* mutants. Similar effect was not observed when FAT-1 or FAT-5 was depleted (Supplementary Figure S4B).

To determine the tissues from which fatty acyl-CoA desaturases modulated the phenotypes of *seip-1(-)* worms, we repeated our experiments with strains that restricted RNAi to the intestine or germline (Melo and Ruvkun, 2012; Cao et al., 2019; Zou et al., 2019). In *seip-1(-)* mutant background, intestine-specific depletion, but not germline-specific depletion, of FAT-2, FAT-3, or FAT-4 enhanced the embryonic arrest phenotype (Figures 4D, Supplementary Figure S4D). Therefore, the synthesis of PUFAs and their derivatives (such as phospholipids and lipoproteins) in the intestine appears to regulate permeability barrier formation by germline factors. We also investigated the dependence on fatty acyl-CoA

desaturases for embryonic development in otherwise wild-type worms. By analyzing the distribution of a yolk protein marker, VIT-2::GFP, we found abnormal accumulation of GFP signals in the pseudocoelom of *fat-3* knockdown worms (Supplementary Figures S6C–E), suggesting a partial block of yolk protein transport into the germline. Interestingly, embryonic arrest was observed only when FAT-2 was depleted ubiquitously in wild type worms (Supplementary Figure S4C). However, neither intestine- nor germline-specific knockdown of *fat-2* recapitulated phenotypes observed when *fat-2* was knocked down ubiquitously. Our results imply that FAT-2 products made in one tissue can diffuse to other tissues to compensate for local FAT-2 deficiency. Based on the differential requirement of fatty acyl-CoA desaturases in wild type and *seip-1(-)* worms, different PUFAs and their derivatives appear to contribute to germline and embryonic development in multiple ways, including but not limited to the establishment of ER subdomains and intestine-to-germline lipid transport. The distribution of these PUFA derivatives in specific membranes and vesicles will require further chemical analysis.

PLIN-1 Deficiency Rescues the Embryonic Defect of *seip-1(-)* Mutants

We inadvertently discovered that PLIN-1 inhibited an alternative mechanism that supported permeability barrier formation in *seip-1(-)* worms. In an attempt to tag all isoforms of PLIN-1 with the mRuby red fluorescent protein, we inserted the mRuby coding sequence to the 5' end of the *plin-1* gene by CRISPR (Supplementary Figure S5A). When we introduced the resultant allele, *hj249*, into *seip-1(-)* worms, we were surprised that the fertility of *plin-1(hj249); seip-1(-)* worms was similar to that of wild type worms (Supplementary Figure S5B). Accordingly, the percentage of BODIPY-positive embryos was significantly reduced (Supplementary Figure S5C). These phenotypes were not observed in *plin-1(hj178)* when PLIN-1A and PLIN-1C isoforms were fused at their C-terminus to GFP (Supplementary Figures S5B,C). Such discrepancy led us to speculate that the mRuby fusion to the N-terminus of PLIN-1 compromised its function, and that *hj249* was a hypomorphic *plin-1* allele that rescued SEIP-1 deficient embryos. To prove our hypothesis, we analyzed worms that carried the *plin-1(tm1704)* deletion allele (Xie et al., 2019) (referred to as *plin-1(-)* hereafter). The *plin-1(-)* worms showed normal permeability barrier formation and fertility (Figures 4A,C). Similar to *plin-1(hj249); seip-1(-)* worms, the fertility of *plin-1(-); seip-1(-)* worms was comparable to that of wild type worms, and almost all embryos had an intact permeability barrier as indicated by the lack of BODIPY staining (Figures 4B,C,G). In addition, the *plin-1(-)* allele rescued the embryonic defects of *seip-1(A185P)* mutants (Supplementary Figures S2C,D), suggesting that the suppression by *plin-1(-)* was not restricted to specific *seip-1* loss of function alleles.

Next, we used RNAi to knockdown *plin-1* ubiquitously, or tissue-specifically in the intestine or germline. We found that ubiquitous or germline-specific RNAi against *plin-1* suppressed *seip-1(-)* (Figure 4D). However, intestine-specific RNAi against

plin-1 did not show similar suppression (Figure 4D). As a complementary approach, we expressed *plin-1* in the germline of *plin-1(-); seip-1(-)* worms, with a *sun-1* promoter driven single-copy transgene. These worms showed embryonic defects similar to *seip-1(-)* worms (Supplementary Figures S5B,C). Thus, our results indicate that the loss of PLIN-1 function in the germline is sufficient to bypass the requirement on SEIP-1 for permeability barrier formation. Interestingly, ubiquitous knockdown of *fat-2* or *fat-3* and intestine-specific knockdown of *fat-3* by RNAi reversed the suppression of *seip-1(-)* associated embryonic defects by *plin-1(-)* (Figure 4E, Supplementary Figure S4E). Therefore, *plin-1(-); seip-1(-)* worms appeared to rely on FAT-2 or FAT-3, acting in distinct tissues, to support permeability barrier formation. Our results support the notion that local and diffusible PUFAs and their derivatives are required for embryonic development of *C. elegans*.

RAB-18 is Required for the Development of *seip-1(-); plin-1(-)* Embryos

Next, we sought to identify proteins that acted redundantly with SEIP-1 to ensure embryonic development. To this end, we inactivated genes encoding known or putative LD-associated proteins by RNAi. We found that ubiquitous or germline-specific *rab-18* knockdown yielded BODIPY-positive, permeability barrier defective *plin-1(-); seip-1(-)* embryos (Figure 4E). Intestine-specific RNAi against *rab-18* had no effect (Figure 4E). Similar observations were made when *dgtr-1*, a gene known to be essential for permeability barrier formation (Olson et al., 2012), was knocked down in *plin-1(-); seip-1(-)* embryos (Figure 4E). Our results suggest that RAB-18 acts in the germline, in the absence of SEIP-1, to support permeability barrier formation in a DGTR-1-dependent manner. It should be noted that loss of *dgtr-1* function caused highly penetrant embryonic arrest of otherwise wild type worms (Carvalho et al., 2011). In contrast, worms harboring the *rab-18(ok2020)* [referred to as *rab-18(-)* hereafter] loss of function allele did not arrest as embryos and produced comparable number of live progenies as wild type worms (Figure 4F). However, loss of *rab-18* significantly increased the percentage of arrested embryos from *plin-1(-); seip-1(-)* worms and reduced the number of live progenies accordingly (Figures 4F,G). Using CRISPR, we also generated a mutant *rab-18* allele that encoded the S25N mutation (Supplementary Figure S7A). The S25N mutation is analogous to S22N of human Rab18, which “locks” RAB-18 in a constitutively GDP-bound form. Based on BODIPY staining, we found that the *seip-1(-); plin-1(-); rab-18(S25N)* mutants shared the same permeability barrier defect as *plin-1(-); seip-1(-); rab-18(-)* mutants (Supplementary Figure S7B). Our results imply that active RAB-18 is specifically required in *plin-1(-); seip-1(-)* worms to support embryonic development.

To elucidate the mechanism by which RAB-18 supported permeability barrier formation in the absence of SEIP-1 and PLIN-1, we investigated the localization of GFP::RAB-18 fusion protein, expressed from its endogenous locus (Supplementary Figure S7A). It did not localize to distinct structures in wild type and *plin-1(-)* worms (Figures 4H,I). In *seip-1(-)* worms, GFP::

RAB-18 appeared in numerous diffraction-limited puncta throughout the cytoplasm of newly fertilized (+1, +2) embryos (Figure 4J). Finally, in *plin-1(-); seip-1(-)* embryos, GFP::RAB-18 was found on the LD surface as confirmed by the LDP-1::mRuby marker (Na et al., 2015) (Figures 4K,L). Interestingly, Rab18 supports lipid droplet growth only in the absence of seipin in human A431 cells (Salo et al., 2019). Furthermore, ADRP/Perilipin 2 and Rab18 appeared to compete for LD surface association in cultured mammalian cells (Ozeki et al., 2005). Therefore, it was plausible that the loss of PLIN-1 in *seip-1(-)* embryos similarly permitted the association of RAB-18 with LDs that contained the cargos for permeability barrier construction. Taken together, our results support the notion that RAB-18 positive LDs assume an identity that is similar to SEIP-1 (+) LDs in otherwise wild type embryos. The association of RAB-18 with LDs is modulated by other resident LD proteins, such as PLIN-1.

Minor Contribution of Lipolysis to the Development of *seip-1(-); plin-1(-)* Embryos

Because perilipin orthologs are best known for their role in regulating lipolysis (Supplementary Figure S7C), we asked if basal lipolysis contributed to the high percentage survival of *plin-1(-); seip-1(-)* embryos. Using multiple independent deletion alleles (Supplementary Figure S7A), we found that loss of ATGL-1/ATGL, but not LID-1/CGI-58 or HOSL-1/HSL, partially reduced the survival of *plin-1(-); seip-1(-)* embryos (Supplementary Figures S7D,E). However, the percentage of arrested *plin-1(-); seip-1(-); atgl-1(-)* embryos was lower than that of *plin-1(-); seip-1(-); rab-18(-)* embryos. We also noted that ATGL-1 was already present on lipid droplets in *plin-1(-)* single mutants (Supplementary Figures S7F,G), whereas RAB-18 was present on lipid droplets specifically in *plin-1(-); seip-1(-)* mutants (Figure 4K). Taken together, we conclude that ATGL-1 and RAB-18 may contribute separately to permeability barrier formation, and that RAB-18 is more critically required by *plin-1(-); seip-1(-)* mutants.

CONCLUDING REMARKS

In this paper, we used genetic and imaging approaches to reveal a requirement for SEIP-1 in the formation of the permeability barrier, which is part of the *C. elegans* eggshell. Our results suggest that SEIP-1 (+) LDs contribute to the packaging and release of lipid-rich ascarosides that are eventually exported to the embryonic extracellular space. This hypothesis is compatible with the model that embryonic cortical granules are responsible for the export of additional material that constitutes the protein-rich layers of the eggshell (Bembenek et al., 2007; Sato et al., 2008; Kimura and Kimura, 2012). We propose that the ability of SEIP-1 to mark a subset of mature LDs is separable from its other established function in supporting the emergence of nascent LDs from the ER (Chung et al., 2019; Salo et al., 2019; Prasanna et al., 2021; Zoni et al., 2021). It is plausible that SEIP-1 enrichment to ER

subdomains promotes the assembly of enzymes that are required for ascarosides synthesis, prior to their deposition into specialized LDs. Future efforts will be needed to determine the localization of the full set of germline factors that contribute to the permeability barrier formation. It is well-established that mammary epithelial cells export milk fat in the form of LDs (Masedunskas et al., 2017). Interestingly, seipin knockout mice are defective in milk production and lactation (El Zowalaty et al., 2018). Therefore, it is tempting to speculate that the involvement of seipin-positive LDs in the export of lipophilic molecules may be a conserved phenomenon. Our discovery that PLIN-1 deficiency can suppress and FAT-3 deficiency can enhance the *seip-1(-)* embryonic arrest phenotype suggests that parallel pathways exist to permit 'alternative' LDs to accommodate and release ascarosides (Figure 4M). Taken together, we propose that the plasticity of the LD surface coat supports a safety mechanism that ensures the construction of the permeability barrier, which is crucial for *C. elegans* eggshell integrity and embryo survival *ex utero*.

METHODS AND MATERIALS

Strains and Transgenes

Bristol N2 was used as the wild-type *C. elegans* strain. All animals were maintained and investigated at 20°C. The following alleles and transgenes were obtained from the Caenorhabditis Genetics Center (CGC): *LG III, unc-119 (ed3), rab-18 (ok2020), tIs38 [(pAA1)pie-1p::GFP::PH (PLC1delta1) + unc-119(+)]*; *LG IV, fat-3 (ok1126)*; *LG V, sid-1 (qt78), tIs44 [(pAA173)pie-1p::mCherry::PH (PLC1delta1) + unc-119 (+)]*; *LG X, vit-2 (crg9070)*. *seip-1 (tm4221) V* and *plin-1 (tm1704) I* alleles were obtained from Dr. Shohei Mitani (National Bioresource Project for the nematode). *rde-1 (mkc36) V* and *mkcSi13 [sun-1p::rde-1::sun-1 3' UTR] II* are gifts from Dr. Di Chen (Model Animal Research Center, Nanjing University). The following single-copy transgenes were used: *hjSi3 [vha-6p::seip-1 cDNA::GFP_TEV_3x-FLAG::let-858 3' UTR] II*, *hjSi189[dpy-30p::seip-1 cDNA::GFP_TEV_3xFLAG::tbb-2 3' UTR] II*, *hjSi206 [vha-6p::human seipin isoform 2 cDNA (codon optimized)::GFP_TEV_3xFLAG::let-858 3' UTR] II*, *hjSi223[dpy-30p::human seipin isoform 2 cDNA (codon-optimized)::GFP_TEV_3xFLAG::tbb-2 3' UTR] II*, *hjSi434[dpy-30p::seip-1 cDNA::tagRFP::tbb-2 3' UTR] II*, *hjSi494[vha-6p::sid-1 cDNA::dhs-28 3' UTR] I*, *hjSi502[sun-1p::seip-1 cDNA::GFP_TEV_3xFLAG::sun-1 3' UTR] II*, *hjSi541[dyp-30p::seip-1(A185P) cDNA::GFP_TEV_3xFLAG::tbb-2 3' UTR] II*, *hjSi552[sun-1p::plin-1 gDNA::GFP_TEV_3xFLAG::sun-1 3' UTR] II*. The following CRISPR/Cas9-generated alleles were used: *hj140[seip-1::GFP_TEV_3xFLAG] V*, *hj158[seip-1(A185P)::stop codon_loxP_seip-1 3'-UTR] V*, *hj178[plin-1a/c::GFP_TEV_3xFLAG] I*, *hj249 [mRuby_TEV_3xFLAG::plin-1] I*, *hj256[sec-16A.1::GFP_TEV_3xFLAG] III*, *hj289[ldp-1::mRuby_TEV_3xHA] V*, *hj323 [seip-1::mKikGR_SEC_3xFLAG] V*, *hj340[cpg-2 signal peptide::mCherry_TEV_3xFLAG::cpg-2 w/o signal peptide] III*, *hj345 [GFP_TEV_3xFLAG::atgl-1] III*, *hj347[GFP_TEV_3xFLAG::rab-18b] III*, *atgl-1 (hj349, hj352) III*, *lid-1 (hj355, hj358) I*, *hosl-1 (hj360, hj361) X*, *hj371[GFP_TEV_3xFLAG::rab-18b(S22N)] III*.

The sgRNA sequences for CRISPR are listed in **Supplementary Table S2**.

RNA Interference-Based Knockdown in *C. elegans*

RNA interference (RNAi) was performed by on-plate feeding according to published methods (Neve et al., 2020). The targeting sequence in each RNAi vector was either taken from the Ahringer library or constructed with primers detailed in **Supplementary Table S1**. The plasmids were transformed into OP50 [rnc14::DTn10 lacZgA::T7pol camFRT] (Neve et al., 2020). Fresh overnight cultures of OP50 RNAi clones were seeded on NGM plates with 0.4 mM IPTG and 100 µg/ml Ampicillin. The seeded plates were stored in the dark and incubated at room temperature for 1 day prior to experiments. The intestine-specific and germline-specific knockdown was performed as previously described (Cao et al., 2019; Zou et al., 2019). In brief, the single-copy intestine-specific (*hjSi494*) or germline-specific (*mkcSi13*) transgene is used to rescue *sid-1(qt78)* or *rde-1(mkc36)* mutant animals, respectively. The *seip-1(tm4221)* and/or *plin-1(tm1704)* allele were introduced into *hjSi494*; *sid-1 (qt78)* and *mkcSi13*; *rde-1(mkc36)* by genetic crosses. Further details of the RNAi clones can be found in **Supplementary Table S1**.

Fluorescence Imaging of *C. elegans*

For all fluorescence imaging, one-day-old adult animals were examined by a spinning disk confocal microscope (AxioObserver Z1, Carl Zeiss) with a ×5 (numerical aperture (NA) 0.16) or ×63 (numerical aperture (NA) 1.4 oil) Alpha-Plan-Apochromat objective. Image stacks were acquired with a Neo sCMOS camera (Andor) and a piezo Z stage controlled by the iQ3 software (Andor). For GFP, a 488 nm laser was used for excitation and emitted signals were collected by a 500–550-nm filter. For mCherry, mRuby, tagRFP, and photo-converted mKikGR, a 561 nm laser was used for excitation and emitted signals were collected by a 580.5–653.5-nm filter. Optical sections of images at 0.5 µm intervals were exported to Imaris 8 (Bitplane) for processing and 3D reconstruction.

For imaging the germline and embryos of live *C. elegans*, fresh 8% agarose pads were prepared on top of microscope glass slides. 2–3 µl of 1.25% (w/v) polystyrene microspheres (Polybead Microspheres 0.05µm, Polysciences) and 0.2 mM levamisole (Sigma) in 1 × PBS were dropped at the center of the agarose pads for immobilization of adult animals. For imaging the permeability barrier, on 22 mm × 22 mm cover slips, embryos were dissected from the uterus of one-day-old adults (24 h after the mid-L4 larval stage) in 0.8 × egg buffer with 0.2 mM levamisole in spherical micro-chambers bordered by vaseline. The microscope glass slides were subsequently applied with care to avoid the compression of the embryos.

For photoconversion of mKikGR, individual plates of one-day-old *seip-1(hj323)* adults (24 h after the mid-L4 larval stage) were exposed to 400–440 nm fluorescence filtered by SZX2-FBV (Olympus) for 30 min on a stereomicroscope (SZX16, Olympus) equipped with a LED light source (EXFO). Worms were allowed

to rest for 1 h at 20°C so that -1 oocytes were ovulated and fertilized prior to confocal microscopy.

Analysis of Fluorescence Images

The diameter of LDs present in -1 oocyte and +1 embryos was manually fitted using the spot function in Imaris. The shortest distance between peri-LD cages and plasma membrane was computed by the spot and surface functions of Imaris XT.

Measurement of Total Number of Live Progenies

Animals carrying the *seip-1(tm4221)* allele were backcrossed four times with wild-type males right before measurement. L4 larval P0 animals of each genotype were singled to individual plates and transferred to new plates every 24–48 h until egg-laying ceased. Hatched F1 animals were monitored and counted 24–48 h after the removal of the P0.

BODIPY-Staining of Embryos

Four one-day-old adults (24 h after the mid-L4 larval stage) per replicate per strain were transferred to a new plate and allowed to lay eggs at 20°C. After 3 hours, adults were removed and the plate was stained with 500 μ l 1 mM BODIPY in 1 \times PBS for 3 h. The percentage of BODIPY-positive embryos was calculated using a fluorescence stereomicroscope. For comparison upon knockdown of different genes, the setup was similar as described above except that the age of adults varied in order to ensure both the efficiency and specificity of the knockdown. For constitutive knockdown, L4 larval P0 animals were plated and one-day-old F1 animals were used for scoring the percentage of BODIPY-positive embryos. For intestine-specific knockdown, L4 larval animals were plated and scored 48 h later. For germline-specific knockdown, L4 larval animals were plated and scored 24 h later.

Generation of Knock-In/Knock-Out Alleles in *C. elegans*

Tagging of the endogenous genes was performed as described previously (Dickinson et al., 2015). In brief, single guide RNAs (sgRNAs, detailed in **Supplementary Table S2**) were designed using CHOPCHOP (<https://chopchop.rc.fas.harvard.edu/>) and cloned into pDD162 (Addgene). The sgRNA/Cas9 vectors were injected into adult *C. elegans* along with the corresponding repair templates and co-injection markers. The transgenic P0s were singled and their progeny were selected with 5 mg/ml hygromycin B (InvivoGen). Viable F2s were further screened using a fluorescence stereomicroscope and PCR-based genotyping to verify knock-in alleles. For knocking out a target gene, 2–4 sgRNAs were injected along with co-injection markers. F1s from the transgenic P0s were singled and genotyped for deletion. For each knock-in/knock-out strain, at least two independent alleles were acquired and examined for consistency. All constructed alleles were backcrossed two times with wild-type males before further characterization.

DATA AVAILABILITY STATEMENT

The raw data supporting the conclusions of this article will be made available by the authors, without undue reservation.

AUTHOR CONTRIBUTIONS

ZC and CWF were responsible for Figures 1A,B, 4C–G, Supplementary Figure S2C,D, S3D,E, S5, S7D,E. ZC was responsible for Figures 1C–J, 2, 3, 4A,B,H–M, Supplementary Figures S1A–C, S2A,B,E–G, S3A–C,F–H, S4, S5A, S6, S7A,C,F–J, and Supplementary Videos. CF was responsible for Supplementary Figures S1D, S7B. ZC and HYM wrote the paper.

FUNDING

The work was supported by RGC GRF 16102118 and 16101820 to HYM.

ACKNOWLEDGMENTS

We thank Yan Hao and Joshua Fung for preliminary data. Di Chen, Meng Wang and King L. Chow for RNAi-related strains and reagents. Jihong Bai, Christian Frøkjær-Jensen and Bob Goldstein for Mos1 and CRISPR reagents. Some strains were provided by the CGC, which is funded by NIH Office of Research Infrastructure Programs (P40 OD010440).

SUPPLEMENTARY MATERIAL

The Supplementary Material for this article can be found online at: <https://www.frontiersin.org/articles/10.3389/fcell.2022.856474/full#supplementary-material>

Supplementary Figure S1 | SEIP-1 supports eggshell integrity of *C. elegans*. **(A)** A schematic diagram summarizing the eggshell composition of wild-type *C. elegans*. The design of the *mCherry::3xFLAG::cpg-2* knockin allele is also shown. **(B)** Comparison of number of eggs laid by wild type (WT) and *seip-1(-)* animals. At least 10 animals of each genotype were scored. Median with interquartile range is shown (applies to all subsequent bar charts and scatter plots). **(C)** The percentage of BODIPY-stained embryos produced by individual *seip-1(-)* adult during the egg-laying period. 20 animals were monitored. **(D)** The percentage of BODIPY-stained embryos produced by animals of the indicated genotype, quantified in a defined time window. Five independent biological samples were scored, each with progeny from four 1-day-old adults. For detailed experimental setup, refer to Methods and Materials.

Supplementary Figure S2 | Animals that express SEIP-1(A185P) phenocopy *seip-1(-)* mutants. **(A)** Sequence alignment of *C. elegans*, *Drosophila*, *S. cerevisiae*, and human seipin orthologs. The human lipodystrophy-associated A212P mutation in seipin is equivalent to A185P in *C. elegans* SEIP-1. **(B)** Schematic representation of specific mutations introduced to the endogenous *seip-1* locus. The two alleles, *hj156* and *hj158*, were engineered by CRISPR/Cas9-mediated HDR with repair templates that only differ at the coding sequence of A185. A loxP scar was left between the stop codon and 3'-UTR of *seip-1* as a result of removing the self-excising cassette (SEC). **(C)** The total number of live progenies from individual animals. At least 10 animals of each genotype were scored. Groups that do not share the same letters are significantly different (ordinary one-way ANOVA with Turkey's multiple comparisons test, $p < 0.01$). **(D)** As in **(C)**, but with the percentage

of BODIPY-stained embryos quantified in a defined time window. Five independent repeats were scored, each with progeny from four 1-day-old adults. Data of the control groups in (C), (D) were reproduced from Figure 1A,B as the measurement was all performed at the same time. (E) Visualization of LDs using PLIN-1::GFP (*hj178*) in 1-day-old *seip-1(hj156)* (control) adults. mCherry::PH(PLC1 δ 1) (*itls44*) labels PM in the germline. mCherry and GFP are pseudocolored magenta and cyan, respectively. Dotted lines mark the boundary between different tissues or embryos. Boxed regions were magnified 5x and displayed at the bottom. A projection of 4.5 μ m z stack reconstituted from 10 focal planes is shown. For anatomical positions of the ROI, refer to Figure 2A. (F) As in (E), but with *seip-1(hj158)* (A185P). Arrows point to aberrantly enlarged LDs. (G) Average diameter of the largest (crimson) or smallest (navy-blue) five LDs in individual 1-day-old adults. At least 10 animals of each genotype were scored. In both oocytes and embryos, when compared to control, the difference between crimson and navy-blue dots is further augmented in *seip-1(A185P)*.

Supplementary Figure S3 | Localization of SEIP-1 in the germline. (A) Visualization of transgenic wild-type SEIP-1::GFP (*hjSi189*) in 1-day-old *seip-1(-)* adults. GFP is pseudocolored cyan. Dotted lines mark the boundary between different tissues or embryos. Boxed regions were magnified 3x and displayed in the inset. A projection of 4.5 μ m z stack reconstituted from 10 focal planes is shown. For anatomical positions of the ROI, refer to Figure 2A. (B) As in (A), but with transgenic SEIP-1(A185P)::GFP (*hjSi541*). (C) As in (A), but with transgenic human *seipin*::GFP (*hjSi223*). (D) The total number of live progenies from individual animals. At least 10 animals of each genotype were scored. Groups with different letters are significantly different (ordinary one-way ANOVA with Turkey's multiple comparisons test, $p < 0.01$). Transgenic SEIP-1::tagRFP is expressed from the single-copy transgene *hjSi434*. (E) As in (D), but with the percentage of BODIPY-stained embryos quantified in a defined time window. Five independent repeats were scored, each with progeny from four 1-day-old adults. (F) Schematic representation of endogenously tagged *sec-16A.1* (*hj256*). All isoforms of SEC-16A.1 are fused with C-terminal GFP in *hj256*. (G) Visualization of SEIP-1::tagRFP (*hjSi434*) and SEC-16A.1::GFP (*hj256*) in a 1-day-old *seip-1(-)* adult. tagRFP and GFP are pseudocolored magenta and cyan, respectively. Single focal planes are shown. Dotted lines mark the boundary between different tissues or embryos. Boxed regions were magnified 5x and displayed at the bottom. (H) As in (G), but with an animal that expressed SEIP-1::tagRFP and VIT-2::GFP (*crg9070*).

Supplementary Figure S4 | Somatic fatty acyl-CoA desaturases contribute to eggshell integrity. (A) The biosynthetic pathway of polyunsaturated fatty acids (PUFAs) in *C. elegans*. (B) The percentage of BODIPY-stained embryos in a defined time window upon constitutive depletion of each gene. Five independent replicates were performed, each with progeny from four 1-day-old *seip-1(-)* adults. Statistical significance on top of each bar is calculated by comparing with the control group (one-way ANOVA with Dunnett's multiple comparisons test). ns, not significant; **** $p < 0.0001$. (C) As in (B), but with individual genes knocked down in the specified tissues of one-day-old wild-type adults. Statistical significance on top of each bar was calculated by comparing each experimental group with its counterpart in the control group (RNAi vector) (two-way ANOVA and Sidak's multiple comparisons test). (D) As in (C), but with *seip-1(-)* adults. (E) As in (D), but with *plin-1(-)*; *seip-1(-)* adults.

Supplementary Figure S5 | The mRuby::PLIN-1 fusion protein is not fully functional. (A) Schematic representation of the modified *plin-1* locus by CRISPR/Cas9. All isoforms of PLIN-1 are fused with mRuby at the N-terminus in animals that carry the *plin-1(hj249)* allele. (B) The total number of live progenies from individual animals. At least 10 animals of each genotype were scored. Groups with different letters are significantly different (ordinary one-way ANOVA with Turkey's multiple comparisons test, $p < 0.01$). Germline rescue of *plin-1(-)* was performed by expressing PLIN-1::GFP from a single-copy transgene, driven by the *sun-1* promoter (*hjSi552*). (C) As in (B), but with the percentage of BODIPY-stained

embryos quantified in a defined time window. Five independent repeats were scored, each with progeny from four 1-day-old adults. Data of the control groups in (B), (C) were reproduced from Figure 1A,B as the measurement was all performed at the same time.

Supplementary Figure S6 | FAT-3 deficiency disrupts SEIP-1 localization and yolk protein transport. (A) Visualization of endogenous SEIP-1::GFP (*hj140*) in wild-type oocytes. The GFP signal is pseudocolored cyan. Dotted lines mark the boundary between different tissues or oocytes. Boxed regions were magnified 3x and displayed in the inset. A projection of 4.5 μ m z stack reconstituted from 10 focal planes is shown. (B) As in (A), but in *fat-3(ok1126)* mutant background. (C) Visualization of VIT-2::GFP (*crg9070*) and the germline-specific plasma membrane marker mCherry::PH(PLC1 δ 1) (*itls44*) in a wild-type one-day-old adult with control RNAi knockdown. The image was stitched from 10 single focal planes of different xy positions. The boxed region was magnified 3x and shown on the side. (D) As in (C), but with a worm subjected to ubiquitous *seip-1* knockdown. (E) As in (A), but with a worm subjected to ubiquitous *fat-3* knockdown. VIT-2::GFP in the pseudocoelom is indicated by a white arrow.

Supplementary Figure S7 | Minor contribution of lipolysis to the development of *seip-1(-)*; *plin-1(-)* embryos. (A) Schematic representation of knock-in or mutant alleles used in Figure 4 and S7. (B) The percentage of BODIPY-stained embryos quantified in a defined time window. Five independent repeats of each genotype were scored, each stemming from four 1-day-old adults. Groups that do not share the same letters are significantly different (ordinary one-way ANOVA with Turkey's multiple comparisons test, $p < 0.01$). (C) A schematic summary of the first two steps of lipolysis. (D) The total number of live progenies from individual animals. At least 10 animals of each genotype were scored. Groups that do not share the same letters are significantly different (ordinary one-way ANOVA with Turkey's multiple comparisons test, $p < 0.01$). (E) As in (D), but with the percentage of BODIPY-stained embryos quantified in a defined time window. Five independent biological samples were scored, each stemming from four 1-day-old adults. Data of the control groups in (D), (E) were reproduced from Fig. 1A-B as the measurement was all performed at the same time. (F) Visualization of GFP::ATGL-1 expressed from its endogenous locus (*hj345*) in an otherwise wild-type 1-day-old adult. Dotted lines mark the boundary between different tissues or embryos. Boxed regions were magnified 5x and shown in the inset. GFP is pseudocolored cyan. A projection of 4.5 μ m z stack reconstituted from 10 focal planes is shown. Scale bar = 10 μ m. (G) As in (F), but in *plin-1(-)* mutant background. (H) As in (F), but in *seip-1(-)* mutant background. (I) As in (F), but in *plin-1(-)*; *seip-1(-)* mutant background. (J) Visualization of GFP::ATGL-1 (*hj345*) and LDP-1::mRuby (*hj289*) in an isolated one-cell stage embryo from a 1-day-old *plin-1(-)*; *seip-1(-)* adult. Dotted lines mark the boundary of the embryo. LDP-1::mRuby serves as a LD marker. GFP and mRuby are pseudocolored cyan and magenta, respectively. A single focal plane is shown. The boxed region was magnified 4x and shown at the bottom. Scale bar = 10 μ m.

Supplementary Video S1 | Time-lapse monitoring of the perivitelline space (PVS) marker mCherry::CPG-2 (magenta, *hj340*) with the plasma membrane (PM) marker GFP::PH(PLC1 δ 1) (cyan, *itls38*) in newly fertilized wild-type embryos. Images were acquired *in utero* at 5-sec intervals. Display rate = 10 frames/second.

Supplementary Video S2 | As in Video 1, but in *seip-1(tm4221)* mutant background.

Supplementary Video S3 | Time-lapse monitoring of SEIP-1::tagRFP (magenta, *hjSi434*) with the plasma membrane (PM) marker GFP::PH(PLC1 δ 1) (cyan, *itls38*) in newly fertilized wild-type embryos. The fluorescence signals were merged with bright-field (BF) signals that showed the position of embryos in the uterus. All images were acquired at 5-sec intervals. Display rate = 10 frames/second.

REFERENCES

- Bai, X., Huang, L.-J., Chen, S.-W., Nebenfuhr, B., Wysolmerski, B., Wu, J.-C., et al. (2020). Loss of the Seipin Gene Perturbs Eggshell Formation in *C. elegans*. *Development* 147(20). doi:10.1242/dev.192997
- Bembenek, J. N., Richie, C. T., Squirrel, J. M., Campbell, J. M., Eliceiri, K. W., Poteryaev, D., et al. (2007). Cortical Granule Exocytosis in *C. Elegans* is Regulated by Cell Cycle Components Including Separase. *Development* 134, 3837–3848. doi:10.1242/dev.011361
- Binns, D., Lee, S., Hilton, C. L., Jiang, Q.-X., and Goodman, J. M. (2010). Seipin Is a Discrete Homooligomer. *Biochemistry* 49, 10747–10755. doi:10.1021/bi1013003
- Cao, Z., Hao, Y., Fung, C. W., Lee, Y. Y., Wang, P., Li, X., et al. (2019). Dietary Fatty Acids Promote Lipid Droplet Diversity through Seipin Enrichment in an ER Subdomain. *Nat. Commun.* 10, 2902. doi:10.1038/s41467-019-10835-4
- Cartwright, B. R., and Goodman, J. M. (2012). Seipin: from Human Disease to Molecular Mechanism. *J. Lipid Res.* 53, 1042–1055. doi:10.1194/jlr.R023754
- Carvalho, A., Olson, S. K., Gutierrez, E., Zhang, K., Noble, L. B., Zanin, E., et al. (2011). Acute Drug Treatment in the Early *C. elegans* Embryo. *PLoS One* 6, e24656. doi:10.1371/journal.pone.0024656

- Chen, W.-W., Lemieux, G. A., Camp, C. H., Chang, T.-C., Ashrafi, K., and Cicerone, M. T. (2020). Spectroscopic Coherent Raman Imaging of *Caenorhabditis elegans* Reveals Lipid Particle Diversity. *Nat. Chem. Biol.* 16, 1087–1095. doi:10.1038/s41589-020-0565-2
- Chen, W., Chang, B., Saha, P., Hartig, S. M., Li, L., Reddy, V. T., et al. (2012). Berardinelli-Seip Congenital Lipodystrophy 2/Seipin Is a Cell-Autonomous Regulator of Lipolysis Essential for Adipocyte Differentiation. *Mol. Cell Biol.* 32, 1099–1111. doi:10.1128/MCB.06465-11
- Chung, J., Wu, X., Lambert, T. J., Lai, Z. W., Walther, T. C., and Farese, R. V. (2019). LDAF1 and Seipin Form a Lipid Droplet Assembly Complex. *Developmental Cell* 51, 551–563. e7. doi:10.1016/j.devcel.2019.10.006
- Dickinson, D. J., Pani, A. M., Heppert, J. K., Higgins, C. D., and Goldstein, B. (2015). Streamlined Genome Engineering with a Self-Excising Drug Selection Cassette. *Genetics* 200, 1035–1049. doi:10.1534/genetics.115.178335
- El Zowalaty, A. E., Li, R., Chen, W., and Ye, X. (2018). Seipin Deficiency Leads to Increased Endoplasmic Reticulum Stress and Apoptosis in Mammary Gland Alveolar Epithelial Cells during Lactation†. *Biol. Reprod.* 98, 570–578. doi:10.1093/biolre/i0x169
- Ezcurra, M., Benedetto, A., Sornda, T., Gilliat, A. F., Au, C., Zhang, Q., et al. (2018). *C. elegans* Eats its Own Intestine to Make Yolk Leading to Multiple Senescent Pathologies. *Curr. Biol.* 28, 2544–2556. e5. doi:10.1016/j.cub.2018.06.035
- Fei, W., Shui, G., Gaeta, B., Du, X., Kuerschner, L., Li, P., et al. (2008). Fld1p, a Functional Homologue of Human Seipin, Regulates the Size of Lipid Droplets in Yeast. *J. Cell Biol.* 180, 473–482. doi:10.1083/jcb.200711136
- Fu, D., Yu, Y., Folick, A., Currie, E., Farese, R. V., Tsai, T.-H., et al. (2014). *In Vivo* Metabolic Fingerprinting of Neutral Lipids with Hyperspectral Stimulated Raman Scattering Microscopy. *J. Am. Chem. Soc.* 136, 8820–8828. doi:10.1021/ja504199s
- Goldstein, B., Hird, S. N., and White, J. G. (1993). Cell Polarity in Early *C. elegans* Development. *Development* 119, 279–287. doi:10.1242/dev.119.supplement.279
- Grant, B., and Hirsh, D. (1999). Receptor-mediated Endocytosis in the *Caenorhabditis elegans* Oocyte. *MBoC* 10, 4311–4326. doi:10.1091/mbc.10.12.4311
- Green, R. A., Audhya, A., Pozniakovskiy, A., Dammernann, A., Pemble, H., Monen, J., et al. (2008). Expression and Imaging of Fluorescent Proteins in the *C. elegans* Gonad and Early Embryo. *Methods Cell Biol.* 85, 179–218. doi:10.1016/S0091-679X(08)85009-1
- Habuchi, S., Tsutsui, H., Kochaniak, A. B., Miyawaki, A., and van Oijen, A. M. (2008). mKikGR, a Monomeric Photoswitchable Fluorescent Protein. *PLOS ONE* 3, e3944. doi:10.1371/journal.pone.0003944
- Huelgas-Morales, G., and Greenstein, D. (2018). Control of Oocyte Meiotic Maturation in *C. elegans*. *Semin. Cell Developmental Biol.* 84, 90–99. doi:10.1016/j.semcdb.2017.12.005
- Ibayashi, M., Aizawa, R., Mitsui, J., and Tsukamoto, S. (2021). Homeostatic Regulation of Lipid Droplet Content in Mammalian Oocytes and Embryos. *Reprod. Camb. Engl.* 162, R99–R109. doi:10.1530/REP-21-0238
- Johnston, W. L., and Dennis, J. W. (2012). The Eggshell in the *C. elegans* Oocyte-To-Embryo Transition. *Genesis* 50, 333–349. doi:10.1002/dvg.20823
- Kimura, K., and Kimura, A. (2012). Rab6 Is Required for the Exocytosis of Cortical Granules and the Recruitment of Separase to the Granules during the Oocyte-To-Embryo Transition in *Caenorhabditis elegans*. *J. Cell Sci.* 125, 5897–5905. doi:10.1242/jcs.116400
- Magré, J., Delépine, M., Khalouf, E., Gedde-Dahl, T., Van Maldergem, L., Sobel, E., et al. (2001). Identification of the Gene Altered in Berardinelli-Seip Congenital Lipodystrophy on Chromosome 11q13. *Nat. Genet.* 28, 365–370. doi:10.1038/ng585
- Masedunskas, A., Chen, Y., Stussman, R., Weigert, R., and Mather, I. H. (2017). Kinetics of Milk Lipid Droplet Transport, Growth, and Secretion Revealed by Intravital Imaging: Lipid Droplet Release Is Intermittently Stimulated by Oxytocin. *MBoC* 28, 935–946. doi:10.1091/mbc.E16-11-0776
- Melo, J. A., and Ruvkun, G. (2012). Inactivation of Conserved *C. elegans* Genes Engages Pathogen- and Xenobiotic-Associated Defenses. *Cell* 149, 452–466. doi:10.1016/j.cell.2012.02.050
- Mitani, S. (2017). Comprehensive Functional Genomics Using *Caenorhabditis elegans* as a Model Organism. *Proc. Jpn. Acad. Ser. B: Phys. Biol. Sci.* 93, 561–577. doi:10.2183/pjab.93.036
- Molenaar, M. R., Yadav, K. K., Toulmay, A., Wassenaar, T. A., Mari, M. C., Caillon, L., et al. (2021). Retinyl Esters Form Lipid Droplets Independently of Triacylglycerol and Seipin. *J. Cell Biol.* 220, e202011071. doi:10.1083/jcb.202011071
- Mosquera, J. V., Bacher, M. C., and Priess, J. R. (2021). Nuclear Lipid Droplets and Nuclear Damage in *Caenorhabditis elegans*. *Plos Genet.* 17, e1009602. doi:10.1371/journal.pgen.1009602
- Na, H., Zhang, P., Chen, Y., Zhu, X., Liu, Y., Liu, Y., et al. (2015). Identification of Lipid Droplet Structure-Like/resident Proteins in *Caenorhabditis elegans*. *Biochim. Biophys. Acta (Bba) - Mol. Cell Res.* 1853, 2481–2491. doi:10.1016/j.bbamcr.2015.05.020
- Neve, I. A. A., Sowa, J. N., Lin, C.-C. J., Sivaramakrishnan, P., Herman, C., Ye, Y., et al. (2020). *Escherichia coli* Metabolite Profiling Leads to the Development of an RNA Interference Strain for *Caenorhabditis elegans*. *G3 Bethesda Md.* 10, 189–198. doi:10.1534/g3.119.400741
- Olson, S. K., Greenan, G., Desai, A., Müller-Reichert, T., and Oegema, K. (2012). Hierarchical Assembly of the Eggshell and Permeability Barrier in *C. elegans*. *J. Cell Biol.* 198, 731–748. doi:10.1083/jcb.201206008
- Olzmann, J. A., and Carvalho, P. (2019). Dynamics and Functions of Lipid Droplets. *Nat. Rev. Mol. Cell Biol.* 20, 137–155. doi:10.1038/s41580-018-0085-z
- Ozeki, S., Cheng, J., Tauchi-Sato, K., Hatano, N., Taniguchi, H., and Fujimoto, T. (2005). Rab18 Localizes to Lipid Droplets and Induces Their Close Apposition to the Endoplasmic Reticulum-Derived Membrane. *J. Cell Sci.* 118, 2601–2611. doi:10.1242/jcs.02401
- Payne, V. A., Grimsev, N., Tuthill, A., Virtue, S., Gray, S. L., Dalla Nora, E., et al. (2008). The Human Lipodystrophy Gene BSCL2/seipin May Be Essential for normal Adipocyte Differentiation. *Diabetes* 57, 2055–2060. doi:10.2337/db08-0184
- Perez, M. F., Francesconi, M., Hidalgo-Carcedo, C., and Lehner, B. (2017). Maternal Age Generates Phenotypic Variation in *Caenorhabditis elegans*. *Nature* 552, 106–109. doi:10.1038/nature25012
- Prasanna, X., Salo, V. T., Li, S., Ven, K., Vihinen, H., Jokitalo, E., et al. (2021). Seipin Traps Triacylglycerols to Facilitate Their Nanoscale Clustering in the Endoplasmic Reticulum Membrane. *Plos Biol.* 19, e3000998. doi:10.1371/journal.pbio.3000998
- Salo, V. T., Belevich, I., Li, S., Karhinen, L., Vihinen, H., Vigouroux, C., et al. (2016). Seipin Regulates ER-lipid Droplet Contacts and Cargo Delivery. *EMBO J.* 35, 2699–2716. doi:10.15252/embj.201695170
- Salo, V. T., Li, S., Vihinen, H., Hölttä-Vuori, M., Szkalitsity, A., Horvath, P., et al. (2019). Seipin Facilitates Triglyceride Flow to Lipid Droplet and Counteracts Droplet Ripening via Endoplasmic Reticulum Contact. *Developmental Cell* 50, 478–493. e9. doi:10.1016/j.devcel.2019.05.016
- Sato, M., Grant, B. D., Harada, A., and Sato, K. (2008). Rab11 Is Required for Synchronous Secretion of Chondroitin Proteoglycans after Fertilization in *Caenorhabditis elegans*. *J. Cell Sci.* 121, 3177–3186. doi:10.1242/jcs.034678
- Sharrock, W. J., Sutherlin, M. E., Leske, K., Cheng, T. K., and Kim, T. Y. (1990). Two Distinct Yolk Lipoprotein Complexes from *Caenorhabditis elegans*. *J. Biol. Chem.* 265, 14422–14431. doi:10.1016/s0021-9258(18)77319-5
- Stein, K. K., and Golden, A. (2018). The *C. elegans* Eggshell. *WormBook* 2018, 1–36. doi:10.1895/wormbook.1.179.1
- Sui, X., Arlt, H., Brock, K. P., Lai, Z. W., DiMaio, F., Marks, D. S., et al. (2018). Cryo-electron Microscopy Structure of the Lipid Droplet-Formation Protein Seipin. *J. Cell Biol.* 217, 4080–4091. doi:10.1083/jcb.201809067
- Szymanski, K. M., Binns, D., Bartz, R., Grishin, N. V., Li, W.-P., Agarwal, A. K., et al. (2007). The Lipodystrophy Protein Seipin Is Found at Endoplasmic Reticulum Lipid Droplet Junctions and Is Important for Droplet Morphology. *Proc. Natl. Acad. Sci. U.S.A.* 104, 20890–20895. doi:10.1073/pnas.0704154104
- Tagawa, A., Rappleye, C. A., and Aroian, R. V. (2001). Pod-2, along with Pod-1, Defines a New Class of Genes Required for Polarity in the Early *Caenorhabditis elegans* Embryo. *Developmental Biol.* 233, 412–424. doi:10.1006/dbio.2001.0234
- Tauchi-Sato, K., Ozeki, S., Houjou, T., Taguchi, R., and Fujimoto, T. (2002). The Surface of Lipid Droplets Is a Phospholipid Monolayer with a Unique Fatty Acid Composition. *J. Biol. Chem.* 277, 44507–44512. doi:10.1074/jbc.M207712200
- Thul, P. J., Tschapalda, K., Kolkhof, P., Thiam, A. R., Oberer, M., and Beller, M. (2017). Lipid Droplet Subset Targeting of the *Drosophila* Protein CG2254/dmLdsdh1. *J. Cell Sci.* 130, 3141–3157. doi:10.1242/jcs.199661
- Walther, T. C., Chung, J., and Farese, R. V. (2017). Lipid Droplet Biogenesis. *Annu. Rev. Cell Dev. Biol.* 33, 491–510. doi:10.1146/annurev-cellbio-100616-060608
- Wang, H., Becuwe, M., Housden, B. E., Chittraju, C., Porras, A. J., Graham, M. M., et al. (2016). Seipin Is Required for Converting Nascent to Mature Lipid Droplets. *eLife* 5, e16582. doi:10.7554/eLife.16582

- Watson, P., Townley, A. K., Koka, P., Palmer, K. J., and Stephens, D. J. (2006). Sec16 Defines Endoplasmic Reticulum Exit Sites and Is Required for Secretory Cargo Export in Mammalian Cells. *Traffic* 7, 1678–1687. doi:10.1111/j.1600-0854.2006.00493.x
- Welte, M. A. (2015). As the Fat Flies: The Dynamic Lipid Droplets of *Drosophila* Embryos. *Biochim. Biophys. Acta (Bba) - Mol. Cel Biol. Lipids* 1851, 1156–1185. doi:10.1016/j.bbailip.2015.04.002
- Wilfling, F., Wang, H., Haas, J. T., Krahmer, N., Gould, T. J., Uchida, A., et al. (2013). Triacylglycerol Synthesis Enzymes Mediate Lipid Droplet Growth by Relocalizing from the ER to Lipid Droplets. *Developmental Cel* 24, 384–399. doi:10.1016/j.devcel.2013.01.013
- Xie, K., Zhang, P., Na, H., Liu, Y., Zhang, H., and Liu, P. (2019). MDT-28/PLIN-1 Mediates Lipid Droplet-Microtubule Interaction via DLC-1 in *Caenorhabditis elegans*. *Sci. Rep.* 9, 14902. doi:10.1038/s41598-019-51399-z
- Xu, N., Zhang, S. O., Cole, R. A., McKinney, S. A., Guo, F., Haas, J. T., et al. (2012). The FATP1-DGAT2 Complex Facilitates Lipid Droplet Expansion at the ER-Lipid Droplet Interface. *J. Cel Biol.* 198, 895–911. doi:10.1083/jcb.201201139
- Yan, R., Qian, H., Lukmantara, I., Gao, M., Du, X., Yan, N., et al. (2018). Human SEIPIN Binds Anionic Phospholipids. *Developmental Cel.* 9, 248–254.e4. doi:10.1016/j.devcel.2018.09.010
- Zoni, V., Khaddaj, R., Lukmantara, I., Shinoda, W., Yang, H., Schneiter, R., et al. (2021). Seipin Accumulates and Traps Diacylglycerols and Triglycerides in its Ring-like Structure. *Proc. Natl. Acad. Sci. U.S.A.* 118, e2017205118. doi:10.1073/pnas.2017205118
- Zou, L., Wu, D., Zang, X., Wang, Z., Wu, Z., and Chen, D. (2019). Construction of a Germline-specific RNAi Tool in *C. elegans*. *Sci. Rep.* 9, 2354. doi:10.1038/s41598-019-38950-8

Conflict of Interest: The authors declare that the research was conducted in the absence of any commercial or financial relationships that could be construed as a potential conflict of interest.

Publisher's Note: All claims expressed in this article are solely those of the authors and do not necessarily represent those of their affiliated organizations, or those of the publisher, the editors and the reviewers. Any product that may be evaluated in this article, or claim that may be made by its manufacturer, is not guaranteed or endorsed by the publisher.

Copyright © 2022 Cao, Fung and Mak. This is an open-access article distributed under the terms of the Creative Commons Attribution License (CC BY). The use, distribution or reproduction in other forums is permitted, provided the original author(s) and the copyright owner(s) are credited and that the original publication in this journal is cited, in accordance with accepted academic practice. No use, distribution or reproduction is permitted which does not comply with these terms.